Macromolecules
ARTICLE

Macromolecules **2009**, *42*, 8649–8654 **8649**
DOI: 10.1021/ma901609r

Synthesis and Characterization of PMMA/MWNT Nanocomposites Prepared by *in Situ* Polymerization with $Ni(acac)_2$ Catalyst

Liqiang Cui,[†,§] Naresh H. Tarte,[†,‡] and Seong Ihl Woo*[,†,‡]

[†]*Department of Chemical and Biomolecular Engineering, Department of Chemistry and Center for Ultramicrochemical Process System (CUPS), Korea Advanced Institute of Science and Technology, 373-1 Guseong-dong, Yuseong-gu, Daejeon 305-701, Republic of Korea, and* [‡]*Department of Energy Science & Engineering (WCU), Graduate School of EEWS, KAIST, 335Gwahangno, Yuseong-gu, Daejeon 305-701, Republic of Korea.* [§]*Present address: College of Chemical and Environmental Engineering, Shandong University of Science and Technology 579 Qianwangang Road Economic & Technical Development Zone, Qingdao Shandong Province, P. R. China*

Received July 22, 2009; Revised Manuscript Received October 6, 2009

ABSTRACT: Poly(methyl methacrylate)/multiwalled carbon-nanotube (PMMA/MWNT) nanocomposites were prepared via *in situ* polymerization induced by nickel(II) acetylacetonate/methylaluminoxane ([$Ni(acac)_2$]/MAO) catalyst. The incorporation of the MWNT into the PMMA increased the glass transition temperature and thermal decomposition temperature. The solution-casted films of the nanocomposites dissolved in methylene chloride exhibited very high transparency. The introduction of MWNT decreased the syndiotacticity of the resultant PMMA. The storage modulus of the composite increased significantly with increased MWNT content in the PMMA matrix, which was much higher than that of PMMA/clay nanocomposites at the same wt % of filler contents. The PMMA-rich layer which usually formed on the coating surface due to the surface tension and wetting characteristics of the MWNT/PMMA matrix provided excessive interactions between the large surface area nanotubes and the PMMA matrix.

Introduction

Since the discovery of carbon nanotubes (CNT),[1] CNT have been leading to the development of new nanotechnologies because of their exceptional stiffness, strength, and remarkable thermal and electrical properties.[2−5] Since then, significant efforts have been directed toward the fabrication of the polymer/nanotube composites for the development of thermally stable highly conductive material.[6−12] To date, the dispersion of single-wall carbon nanotubes (SWNT) and higher concentrations of multiwall carbon nanotubes (MWNT) into a polymer matrix has been one of the largest challenges. This is because of the large surface areas and van der Waals forces of the CNT which can lead to the formation of strongly bound nanotube aggregates in the resultant polymer nanocomposite.[13]

One of the important goals in nanocomposite fabrication is to enhance the electrical properties, while maintaining the high visible transparency of the nanocomposite material. However, advances in transparent CNT−polymer nanocomposites have been hindered because of the difficulties in achieving high and efficient dispersion, eventually which leads to the low visible transparency. Various methods to obtain homogeneous and fine dispersion of CNT in the polymer are currently being used, including solution mixing in polymer and CNT,[14] a combination of sonication and melt processing,[15] melt blending,[16] and *in situ* polymerization in the presence of nanotubes.[17−22] Nevertheless, developing a much softer and more efficient method to break down the carbon nanotube bundles is still a challenge ahead for the development of the ultimate nanocomposite.

Recently, *in situ* polymerization of ethylene and propylene catalyzed by a highly active metallocene/methylaluminoxane (MAO) complex which is physicochemically anchored onto the carbon nanotube surface has been reported.[23−25] As a result, the CNT were homogeneously coated by the *in situ* grown polyolefin chains, finally leading to the breakdown of the nanotube bundles. The method used was derived from the polymerization-filling technique (PFT) initially investigated in Ziegler−Natta polymerization[26,27] and more recently developed for metallocene catalysis applied to a broad range of microfillers such as kaolin, silica, and graphite.[28−30]

However, until recently there were relatively few reports for the use of such catalysts for homo- and copolymerization of polar monomer. Nickel(II) acetylacetonate/methylaluminoxane [$Ni(acac)_2$/MAO] is an effective catalyst system for methyl acrylate (MMA) polymerization;[31−34] however, the preparation of PMMA/CNT nanocomposite with $Ni(acac)_2$ has never been reported. In this work, the *in situ* polymerization method initiated with a coordination catalyst has been developed first time for the preparation of PMMA/CNT nanocomposite. This approach consists of anchoring cocatalyst (MAO) to the surface of CNT followed by the reaction of the catalyst [i.e., $Ni(acac)_2$] with the MAO-activated CNT. The *in situ* polymerization of MMA catalyzed by this CNT anchored [$Ni(acac)_2$/MAO] leads to the coating of CNT with PMMA and finally breakdown of the nanotube bundles. The structures of the synthesized PMMA/CNT nanocomposites have been investigated; the optical clarity, thermal stability, and mechanical properties of the PMMA/CNT nanocomposites have also been discussed.

Experimental Section

Materials. The MWNT (purity >95%) were supplied by Cheap tubes Inc. (Brattleboro). The diameter of these MWNT is specified as 10−20 nm, and the length is 10−30 μm. To eliminate the impurities present in the MWNT, it was refluxed

*Corresponding author: e-mail siwoo@kaist.ac.kr; Ph +82-42-350-3918; Fax +82-42-350-8890.

Published on Web 10/14/2009

with concentrated nitric acid for 2 h. Finally, it was then repeatedly rinsed with distilled water using a PTFE filter with a pore size of 0.2 μm. MMA (99.9%, Aldrich) was dried with CaH_2 (99.9%, Aldrich) and retrieved by vacuum distillation. Toluene (J.T. Baker) of extra pure grade was purified by refluxing over sodium metal/benzophenone in a nitrogen atmosphere. Nickel(II) acetylacetonate ($Ni(acac)_2$, 95%) purchased from Aldrich was used after sublimation at 140 °C. Anhydrous *n*-heptane (99.9%) was purchased from Aldrich Co. Methylaluminoxane (MMAO-3A, 6.8 wt % in toluene) purchased from Tosoh-Akzo Co. was used as received.

Representative Procedure for Polymerization. *i. Carbon Nanotube Surface Activation.* In a 100 mL polymerization flask, 0.1 g of acid-treated MWNT (c-MWNT) was heated for 8 h at 100 °C under high vacuum. The flask was then inertized using a Schlenk line and placed in an oil bath at 40 °C. Anhydrous *n*-heptane (20 mL) solution of MMAO-3A (10 mL, 20 mmol) was then added to the c-MWNT. The resultant c-MWNTs/MAO mixture was stirred for 1 h at 40 °C. The volatiles were then distilled off at 50 °C under reduced pressure and trapped in a flask cooled by liquid nitrogen. The solidified c-MWNTs/MAO was further heated at 150 °C under high vacuum for 90 min. This c-MWNTs/MAO solid was then directly used in the next step of polymerization.

ii. PMMA/MWNT Nanocomposite Preparation. The polymerization reactions were performed in a 100 mL glass flask. The MAO-treated c-MWNT [c-MWNT/MAO] was dispersed in 30 mL of toluene, and 10 mL of $Ni(acac)_2$ (0.2 mmol) was added to this suspension. After stirring for next 10 min, 10 mL (9.43 g) of MMA monomer was added to the reaction mixture. The polymerization was carried out for 24 h at room temperature with continuous stirring under a inert atmosphere. The reaction was terminated by adding acidified methanol (5% HCl−methanol) solution. The PMMA composites were obtained by precipitation and then dried at 50 °C in a vacuum for 24 h. The yield of PMMA is 4.35 g, and conversion is 45.1% by calculation.

Characterization. The Fourier transform infrared analysis (FT-IR) was obtained at a resolution of 4.0 cm^{-1} using a MAGNA-IR 560 at room temperature. The KBr pellet method was used. Differential scanning calorimetry (DSC) data were obtained with a TA2000 DSC instrument. The representative samples and blank were heated at 10 °C/min up to 200 °C, cooled to 30 °C at 10 °C/min, and finally heated at 10 °C/min to 200 °C. The data discussed herein were taken from the second heating phase of the cycle. Glass transition temperature (T_g) was determined from the midpoint of the step transition in the capacity versus temperature thermogram. Several replicate thermal analyses were carried out for each sample; the data reported are the mean values. The thermal decomposition temperature (T_d) was determined by TGA under nitrogen flow from 40 to 700 °C at the rate of 10 °C/min. Stereoregularities of solvent-extracted PMMA were determined by ^1H NMR analyses (Bruker 500 solution NMR) at room temperature using $CDCl_3$ as *d*-solvent. UV−vis transmission spectra were obtained with a Hitachi U-2000 UV−vis spectrometer. The films of PMMA and PMMA/c-MWNT composites were prepared from a methylene chloride solution by the spin-coating method. Scanning electron microscopy (SEM) analyses were performed with a LEO 1455 VP microscope with samples being coated with gold in a sputter coater. The dynamic properties of the nanocomposites were measured by a Rheometric Scientific DMTA IV with a dual cantilever from 30 to 200 °C with a heating rate of 5 °C/min at a frequency of 1 Hz. The samples were molded into a size of 10 × 30 × 2 mm size at 200 °C for 10 min under a pressure of 4000 psig.

Results and Discussion

In order to eliminate the impurities of MWNT (such as metallic catalysts), it was boiled in concentrated nitric acid for 2 h. At boiling temperature, the concentrated nitric usually produces free oxygen atoms. When such an oxygen atom encounters a carbon nanotube, an oxidation reaction certainly happens. In order to break a nanotube, relatively large numbers of carbon atoms linked together on a nanotube are needed to get oxidized which is rather difficult. However, the end carbon atom of a broken nanotube is more susceptible for oxidation, and hence a carbonyl (⟩C═O) functional group usually generates at the broken end of the nanotubes. Infrared transmission spectra of carbon nanotubes and nitric acid-treated carbon nanotube (c-MWNT) are shown in Figure 1. In the IR spectrum of c-MWNT, characteristic absorptions were observed: the stretching of carboxylic acid group at 1730, 1170, and 1070 cm^{-1}. −OH functional groups appear at 3420 cm^{-1}. It is evident that there are plenty of ⟩C═O and −OH functional groups appearing on the acid-treated MWNT than on original MWNT. These acid-treated MWNT are known to introduce hydroxylic functional groups to MWNT.[35,36] It also makes MWNT more dispersible in common organic solvents.

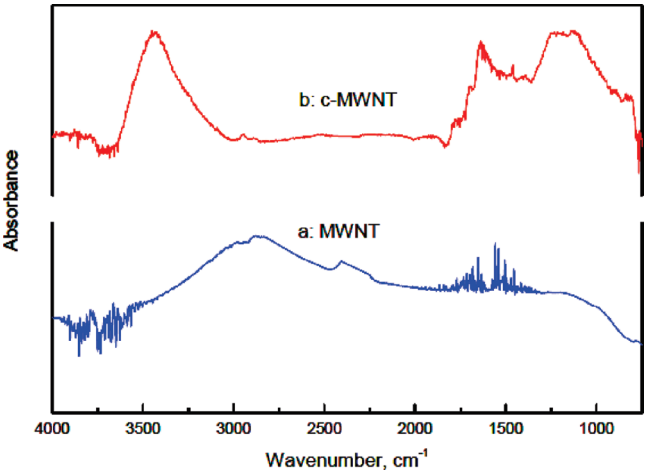

Figure 1. FT-IR spectra of (a) multiwalled carbon nanotube (MWNT) and (b) acid-treated multiwalled carbon nanotube (c-MWNT).

A four-step process of *in situ* polymerization could be described for the preparation of PMMA/c-MWNT composites, as shown in Scheme 1. The steps followed are (1) anchoring MAO onto the MWNT surface, (2) addition of the $Ni(acac)_2$ catalyst onto the surface-activated MWNT, (3) polymerization of MMA onto the MWNT surface, and (4) polymerization and precipitation of PMMA onto the MWNTs. This method finally leads to the breakup of the MWNT bundles and to the efficient dispersion of the MWNT into the PMMA matrix.

After the MAO-activated MWNT had been treated with the $Ni(acac)_2$ catalyst, the MMA monomer was introduced to produce a series of PMMA/c-MWNT composites. The experimental results are listed in Table 1. Under the similar polymerization conditions, increased initial loading of the c-MWNT subsequently increased the c-MWNT contents in the final product. Therefore, this method can vary to some extent the ratio of c-MWNT to PMMA in the final nanocomposites. The percentage of the c-MWNT in the final product determined by TGA measurement is in well agreement with the calculated value using the initial MWNT loading and the polymer yield. The MMA conversion decreased from 78.3% to 45.1% immediately after introducing the c-MWNT into MMA polymerization. However, the conversion of MMA increases from 45.1% to 57.2% with increase of the initial c-MWNT loading. This is because the amount of immobilized MAO onto the c-MWNT increased with increased initial c-MWNT loading. Glass transition temperature (T_g) and thermal decomposition temperature (T_d) of the PMMA/c-MWNT composites obtained from DSC and TGA measurement are listed in Table 1. The pure PMMA exhibits T_g value of

Scheme 1. Scheme of the Polymerization-Filling Technique (PFT) Applied to Multiwalled Carbon Nanotubes

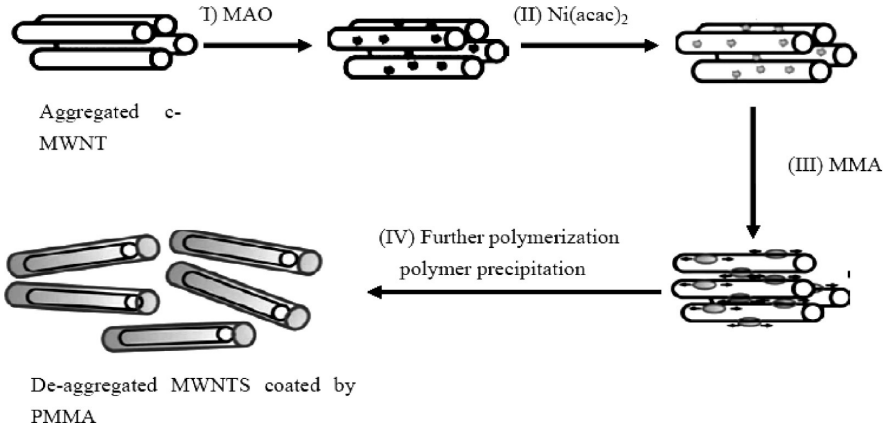

Table 1. Polymerization of Methyl Methacrylate (MMA) with Nickle Acetylacetonate [Ni(acac)$_2$]−Methylaluminoxane (MAO) Supported on Acid-Treated Multiwalled Carbon Nanotube (c-MWNT) System[a]

run no.	initial c-MWNT loading (g)	yield (g)	conv (%)	c-MWNT content in PMMA (wt %)[b]	c-MWNT content in PMMA (wt %)[c]	glass transition temp, T_g (°C)	thermal decompo-sition temp, T_d (5 wt % loss) (°C)	T_d (10 wt % loss) (°C)	electrical conductivity (S/cm)
0	0	7.38	78.3	0	0	119	286	300	
1	0.1	4.35	45.1	2.3	1.8	124	313	334	
2	0.3	4.86	48.4	6.2	4.5	126	318	337	
3	0.5	4.95	47.2	10.1	9.8	128	315	337	4.67×10^{-6}
4	1.0	6.39	57.2	15.6	15.0	129	315	339	1.25×10^{-5}

[a] Polymerization conditions: MMA 10 mL, Ni(acac)$_2$ 0.2 mmol, MMAO-3A 20 mmol as cocatalyst, Al/Ni = 100 (mole ratio); toluene 30 mL as solvent, V_{total} 50 mL, room temperature, 24 h. [b] Calculated using initial MWNT loading and final polymer yield. [c] Determined by TGA.

Table 2. Effect of Multiwalled Carbon Nanotube (MWNT) on Tacticity of Extracted Poly(methyl methacrylate) (PMMA) from PMMA/Acid-Treated Multiwalled Carbon Nanotube (c-MWNT) Composites[a]

				tacticity, %			
run no.	initial c-MWNT loading (g)	extracted by THF 48 h (wt %)	extracted by boiled in THF 48 h (wt %)	rr	mr	mm	T_g (extracted PMMA) (°C)
0	0	92.5	95.3	73.5	18.3	8.2	119
1	0.1	70.5	75.5	55.4	31.5	13.1	116
2	0.3	59.9	62.1	58.8	28.2	13.3	117
3	0.5	23.5	24.9	60.4	22.2	17.4	117
4	1.0	19.4	21.0	60.3	28.3	11.4	117

[a] Polymerization conditions are the same as Table 1.

around 119 °C, which itself is higher than that of PMMA synthesized by radical polymerization.[37] It is due to the difference in PMMA tacticity. As expected, the nanocomposites are characterized by an increase of T_g and T_d (5% and 10% weight loss) with the increased amount of c-MWNT. This can be rationalized by the immobilization of the polymer chains on the surface of treated MWNT and/or by their physical entanglement around the filler which can limit the chain movement. The significant increase in the T_d for the 10% compared to the 5% weight loss can be attributed to the incorporation of c-MWNTs into PMMA which offers a stabilizing effect to the nanocomposite material. Troitskii et al.[38] also reported similar effect during the thermal degradation of PMMA in the presence of C_{60}. The retardation of thermal degradation of PMMA was attributed to interactions between C_{60} and macroradicals generated during the degradation process.

The electrical conductivity of the PMMA/c-MWNT composites increased with the c-MWNT loading from 9.8% to 15.0%. This may be due to the doping effect associated with c-MWNTs which were believed to help induce the formation of a more efficient matrix for charge transport, thus enhancing the electrical conductivity of the composites. However, it is lower than previous reports.[19] The extraction of PMMA from the PMMA/c-MWNT composites was carried out (Table 2) using hot tetrahydrofuran (THF) for 48 h. The PMMA from the PMMA/c-MWNT composites could be partially extracted. Following a similar method, the wt % extraction of PMMA from nanocomposite is far less (20−70%) than the extraction of PMMA from sole PMMA (92.5 wt %). Furthermore, the amount of the extracted PMMA significantly decreases with the increase of the c-MWNT content in the PMMA matrix. The extracted amount of PMMA by Soxhlet extraction method is slightly lower than that of PMMA samples boiled in THF for 48 h.

The effect of c-MWNT on PMMA tacticity was studied by ^{1}H NMR analysis of the extracted PMMA. The results are presented in Table 2 and Figure 2. According to the tacticity data, increased c-MWNT content has great impact on the PMMA tacticity similar to our previous report on PMMA/clay nanocomposite.[33] Introduction of c-MWNT decreased the syndiotacticity from 73.5% for pure PMMA to 55%−60% for PMMA/c-MWNT composites. Because of the anchoring of MAO onto the surface of MWNT, the resultant active site formed on the surface of MWNT restricts the orientation of the monomer, and such hindrance to the monomer insertion can result in the decrease

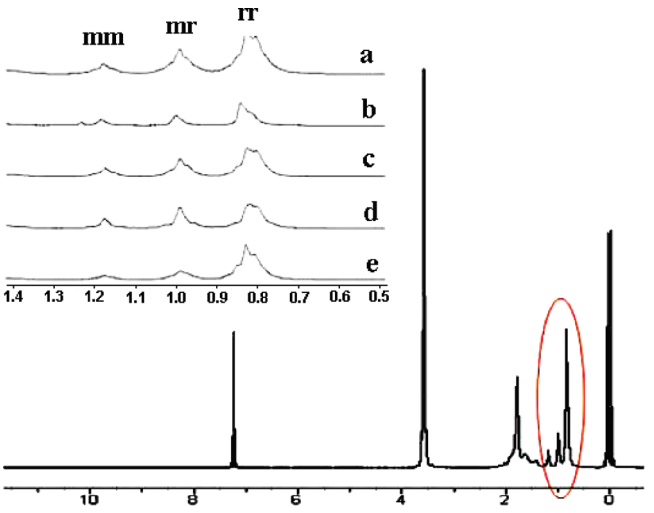

Figure 2. ^{1}H NMR analysis of extracted poly(methyl methacrylate) (PMMA) and poly(methyl methacrylate) (PMMA)/ acid-treated multiwalled carbon nanotube (c-MWNT) nanocomposites: (a) pure PMMA and the PMMA/c-MWNT composites with c-MWNT content of (b) 1.8, (c) 4.5, (d) 9.8, and (e) 15.0 wt %.

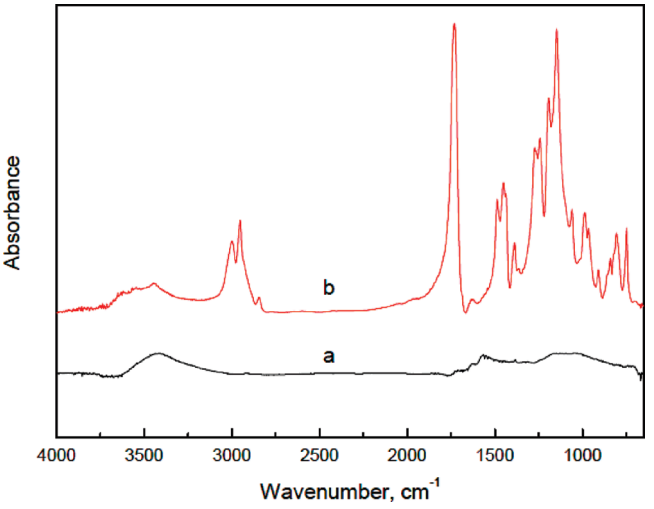

Figure 3. FT-IR spectra of (a) acid-treated multiwalled carbon nanotube (c-MWNT) and (b) poly(methyl methacrylate) (PMMA)/acid-treated multiwalled carbon nanotube (c-MWNT) composites extracted by tetrahedrofuran (THF) (sample run 2).

of syndiotacticity of the PMMA. A similar effect on the PMMA tacticity was also observed in PMMA/clay nanocomposites as separately reported by us[33] and Chung's group.[39] Furthermore, the DSC analyses of the PMMA extracted from the nanocomposite showed slightly lower T_g than that of pure PMMA. This is due to the lowering of syndiotacticity of the extracted PMMA. It reveals that the increase in T_g of PMMA/c-MWNT composites is only due to the better dispersion of MWNT in PMMA matrix and strong interaction between the MWNTs and polymer matrix. The interactions between PMMA and MWNTs have also been studied by FT-IR, as shown in Figure 3.

Figure 3a,b shows FT-IR spectra of the c-MWNT and the THF-extracted PMMA/c-MWNT composite after 48 h of extraction with reflux THF. The two peaks at ~2987 and 2940 cm^{-1} correspond to the C−H stretching bands, which are strengthened after the THF extraction of PMMA/c-MWNT composites. C−H bending band at ~1400 cm^{-1} and C=C stretching band at ~1500 cm^{-1} are clearly seen in Figure 3b. The characteristic peak of C=O of PMMA appeared at ~1735 cm^{-1} is also clearly observed in the curve of the PMMA/c-MWNT after THF

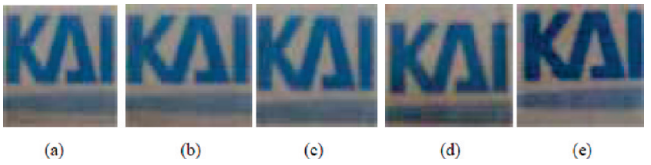

Figure 4. Films of (a) pure poly(methyl methacrylate) (PMMA) and (b−e) PMMA/acid-treated multiwalled carbon nanotube (c-MWNT) composites with different c-MWNT contents [(b) 1.8, (c) 4.5, (d) 9.8, and (e) 15.0 wt %].

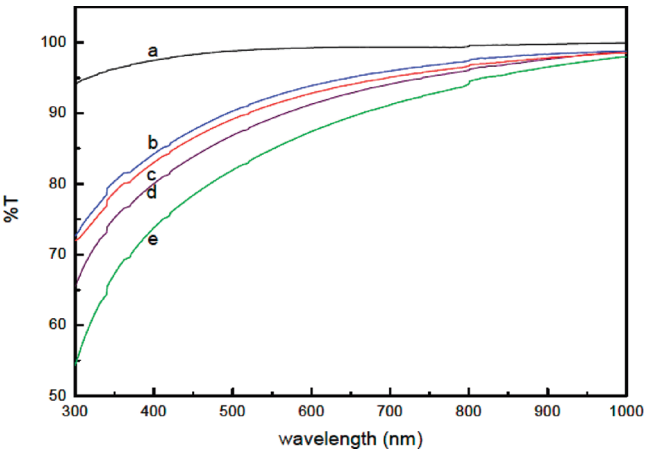

Figure 5. UV−vis spectra of (a) pure poly(methyl methacrylate) (PMMA) and (b−e) PMMA/acid-treated multiwalled carbon nanotube (c-MWNT) composites with different c-MWNT contents [(b) 1.8, (c) 4.5, (d) 9.8, and (e) 15.0 wt %].

extraction. As the residual PMMA/c-MWNTs composites were thoroughly extracted with THF, we believe that there is no free PMMA in the composite, and the presence of PMMA absorptions in the IR spectrum supports the occurrence of a grafting reaction between the PMMA and MWNT. These results show that only part of the PMMA could be extracted from the nanocomposites, and part of the PMMA chains stayed immobilized on the MWNT. This confirms that there exist strong interactions between MWNT and the PMMA segments.

Transparent films with a thickness of 100 nm were produced from a methylene chloride solution of the PMMA/c-MWNT composite with different MWNT amounts, as depicted in Figure 4. The transparence of films decreased with increases of MWNT content in PMMA/c-MWNT composites. As shown in Figure 5, the UV−vis spectra provide quantitative information concerning the transparency of the film, the presence of the MWNTs, and the uniformity of dispersion. The PMMA/c-MWNT nanocomposites show transmission lower than that of the pure PMMA, and transmission of composite films decreases with the increase of c-MWNT amount in PMMA matrix. However, all four composites exhibited a transmittance of 50% and higher in the visible region. It could be associated with different dispersion degrees and abilities of the nanotubes in the polymer framework.

Figure 6 shows the SEM images of both acid-treated MWNT and a fractured surface of PMMA/c-MWNT composite containing 4.5 wt % of MWNT. As shown in the SEM image (Figure 6a), c-MWNT are well distributed in the form of an extended network over a large area, and many entangled clusters of MWNT are observed. Figure 6b shows the presence of segregated MWNT embedded in the PMMA matrix, and smooth interfaces between MWNT and PMMA were observed, so that the MWNT are considered to have good wettability for PMMA. The lack of compatibility may lead to some agglomerated MWNT clusters. However, these entangled clusters were not found on the fractured surface.

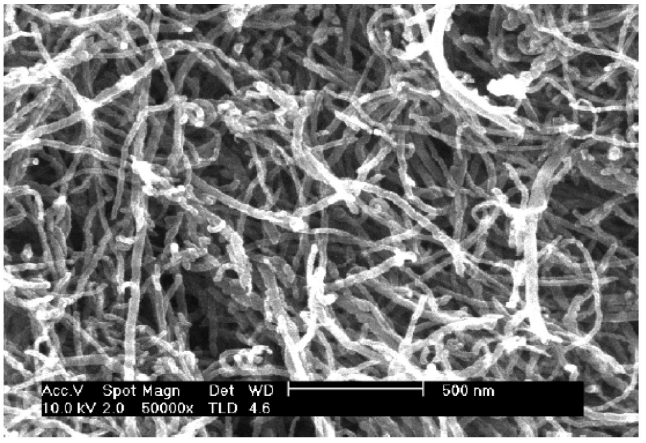

(a)

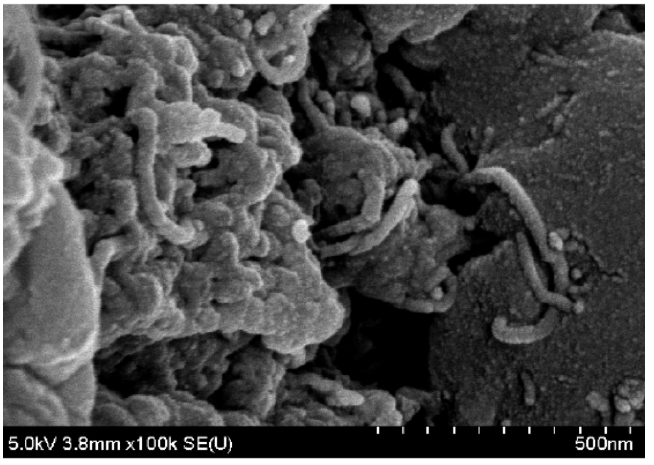

(b)

Figure 6. SEM images of (a) acid-treated multiwalled carbon nanotube (c-MWNT) and (b) poly(methyl methacrylate) (PMMA)/c-MWNT composites (sample run 2).

DMTA can be used to examine the elastic and viscous properties of a polymeric material. The temperature dependence of storage modulus (E') and tan δ are shown in Figures 7 and 8, respectively. Figure 7 shows the storage module of PMMA/c-MWNT composites with different MWNT contents. The storage module of PMMA/c-MWNT composites significantly increased with increasing the amount of c-MWNT in PMMA matrix. The storage modulus of PMMA is increased by the stiffening effect of the nanotubes. In addition, the presence of carbon nanotubes also enables the matrix to sustain a high modulus value to higher temperature. Comparing with our previous work for prepared PMMA/clay nanocomposites (Figure 8a), PMMA/c-MWNT composites have much higher storage module than that of PMMA/clay nanocomposites. It may be attributed to the much higher stiffness and aspect ratio of the CNT compared with that of clay. Figure 8 shows the tan δ peaks of the composites. The peak obviously shifted to the higher temperature with increasing c-MWNT content, showing that the T_g of the composite is raised by the addition of nanotubes. In other words, nanotubes hinder the segmental motion of the PMMA chains. The relation of T_g and the MWNT content in PMMA matrix is consistent with the DSC results.

Conclusions

PMMA/MWNT nanocomposites have been fabricated by *in situ* polymerization technique using the $Ni(acac)_2$/MAO catalyst system. The pretreatment of c-MWNTs with cocatalyst MAO

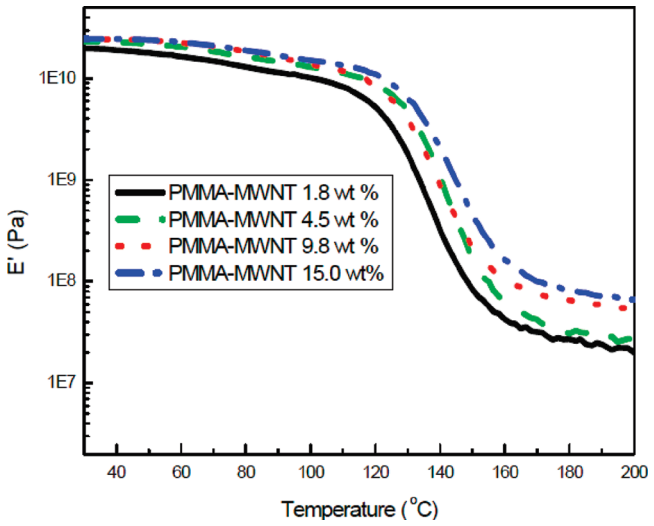

Figure 7. Trend of the storage modulus (E') of poly(methyl methacrylate) (PMMA)/acid-treated multiwalled carbon nanotube (c-MWNT) composites with different c-MWNT contents.

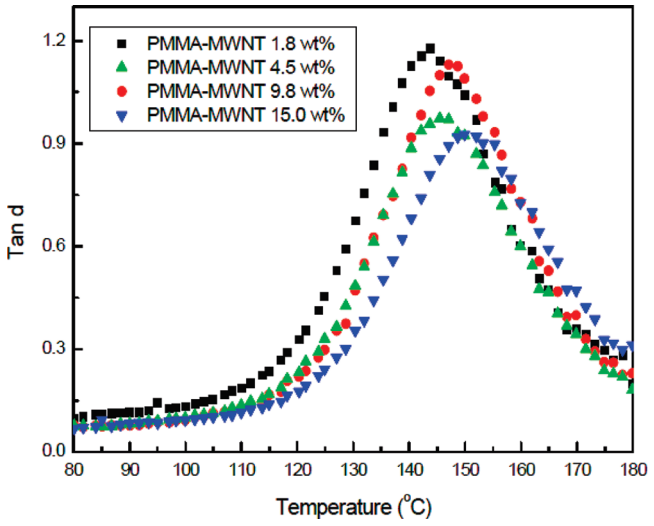

Figure 8. Tan δ vs temperature for pure poly(methyl methacrylate) (PMMA) and PMMA/acid-treated multiwalled carbon nanotube (c-MWNT) composites with different c-MWNT contents.

resulted into the isolation of native carbon nanotube aggregates in comparison with the starting bundlelike associations. It could be seen that the uniformity of the dispersion was dependent on the pretreatment of the MWNT and the polymerization procedure. The incorporation of MWNT into PMMA led to an increase of the glass transition temperature and thermal decomposition temperature of the resultant PMMA nanocomposite. The introduction of MWNT resulted in the lower syndiotacticity of PMMA. The storage modulus of the composite is significantly increased with increase of the MWNT content in PMMA matrix, and it is much higher than that of PMMA/clay nanocomposites at the same filler contents. The tan δ also moved to a higher temperature. It points to a significant improvement of thermal mechanical properties of the PMMA/c-MWNT composites compared to pure PMMA, and hence this is one of the good examples of polymer-based nanocomposite material with enhanced optical and electrical properties.

Acknowledgment. This work was funded by the Center for Ultramicrochemical Process Systems (CUPS) sponsored by KOSEF

(2009) and also funded by WCU Program (31-2008-000-10055-0) funded by MEST (2009).

References and Notes

(1) Iijima, S. *Nature* **1991**, *354*, 56–58.
(2) Ajayan, P. M. *Chem. Rev.* **1999**, *99*, 1787–1800.
(3) Thostenson, E. T.; Ren, Z.; Chou, T. W. *Compos. Sci. Technol.* **2001**, *61*, 1899–1912.
(4) Dai, H. *Acc. Chem. Res.* **2002**, *35*, 1035–1044.
(5) Hirsch, A. *Angew. Chem., Int. Ed.* **2002**, *41*, 1853–1859.
(6) Schadler, L. S.; Giannaris, S. C.; Ajayan, P. M. *Appl. Phys. Lett.* **1998**, *73*, 3842–3844.
(7) Jin, L.; Bower, C.; Zhou, O. *Appl. Phys. Lett.* **1998**, *73*, 1197–1199.
(8) Lozano, K.; Bonilla-Rios, J.; Barrera, E. V. *J. Appl. Polym. Sci.* **2001**, *80*, 1162–1172.
(9) Gong, X.; Liu, J.; Baskaran, S.; Voise, R. D.; Young, J. S. *Chem. Mater.* **2000**, *12*, 1049–1052.
(10) Cooper, C. A.; Ravich, D.; Lips, D.; Mayer, J.; Wagner, H. D. *Compos. Sci. Technol.* **2002**, *62*, 1105–1112.
(11) Kearns, J. C.; Shambaugh, R. L. *J. Appl. Polym. Sci.* **2002**, *86*, 2079–2084.
(12) Potschke, P.; Rosen, R.; Jin, L.; Han, J.; Zhou, O. *Appl. Phy. Lett.* **1999**, *74*, 3317–3319.
(13) Lim, S. T.; Hyun, Y. H.; Choi, H. J.; Jhon, M. S. *Chem. Mater.* **2002**, *14*, 1839–1844.
(14) Shaffer, M. S. P.; Windle, A. H. *Adv. Mater.* **1999**, *11*, 937–941.
(15) Jin, Z.; Pramoda, K. P.; Xu, G.; Goh, S. H. *Chem. Phys. Lett.* **2001**, *337*, 43–47.
(16) Haggenmuller, R.; Gommans, H. H.; Rinzler, A. G.; Fischer, J. E.; Winkey, K. I. *Chem. Phys. Lett.* **2000**, *330*, 219–225.
(17) Park, S. J.; Cho, M. S.; Lim, S. T.; Choi, H. J.; Jhon, M. S. *Macromol. Rapid Commun.* **2003**, *24*, 1070–1073.
(18) Sung, J. H.; Kim, H. S.; Jin, H.-J.; Choi, H. J.; Chin, I.-J. *Macromolecules* **2004**, *37*, 9899–9902.
(19) Park, S. J.; Lim, S. T.; Cho, M. S.; Kim, H. M.; Joo, J.; Choi, H. J. *Curr. Appl. Phys.* **2005**, *5*, 302–304.
(20) Clayton, L. M.; Sikder, A. K.; Kumar, A.; Cinke, M.; Meyyappan, M.; Gerasimov, T. G.; Harmon, J. P. *Adv. Funct. Mater.* **2005**, *15*, 101–106.
(21) Blond, D.; Barron, V.; Ruether, M.; Ryan, K. P.; Nicolosi, V.; Blau, W. J.; Coleman, J. N. *Adv. Funct. Mater.* **2006**, *16*, 1608–1614.
(22) Yao, X.; Wu, H. X.; Wang, J.; Qu, S.; Chen, G. *Chem.—Eur. J.* **2007**, *13*, 846–853.
(23) Bonduel, D.; Mainil, M.; Alexandre, M.; Monteverde, F.; Dubois, P. *Chem. Commun.* **2005**, 781–783.
(24) Kaminsky, W.; Funck, A.; Wiemann, K. *Macromol. Symp.* **2006**, *239*, 1–6.
(25) Bonduel, D.; Bredeau, S.; Alexandre, M.; Monteverde, F.; Dubois, P. *J. Mater. Chem.* **2007**, *17*, 2359–2366.
(26) Enikolopian, N. S. USSR Patent 763 379, **1976**.
(27) Howard, E. G. US Patent 4097447, **1978**.
(28) Kamisky, W.; Zielonka, H. *Polym. Adv. Technol.* **1993**, *4*, 415–422.
(29) Alexandre, M.; Martin, E.; Dubois, P.; Garcia-marti, M.; Jerome, R. *Chem. Mater.* **2001**, *13*, 236–237.
(30) Alexandre, M.; Pluta, P.; Dubois, P.; Jerome, R. *Macromol. Chem. Phys.* **2001**, *202*, 2239–2246.
(31) Coutinho, F. M. B.; Costa, M. A. S.; Monteiro, L. F.; Maria, L. C. S. *Polym. Bull.* **1997**, *38*, 303–309.
(32) Endo, K.; Inukai, A. *Polym. Int.* **2000**, *49*, 110–114.
(33) Cui, L.; Tarte, N. H.; Woo, S. I. *Macromolecules* **2008**, *41*, 4268–4274.
(34) Cui, L.; Tarte, N. H.; Woo, S. I. *J. Appl. Polym. Sci.* **2008**, *110*, 784–790.
(35) Tsang, S. C.; Chen, Y. K.; Harris, P. J. F.; Green, M. L. H. *Nature* **1994**, *372*, 159–162.
(36) Jia, Z.; Wang, Z.; Liang, J.; Wei, B.; Wu, D. *Carbon* **1999**, *37*, 903–906.
(37) Huang, X.; Brittain, W. J. *Macromolecules* **2001**, *34*, 3255–3260.
(38) Troitskii, B. B.; Troitskaya, L. S.; Yakhnov, A. S.; Lopatin, M. O.; Novikova, M. A. *Eur. Polym. J.* **1997**, *33*, 1587–1590.
(39) Choi, S. K.; Choi, M. H.; Wang, K. H.; Kim, S. O.; Kim, Y. K.; Chung, I. J. *Macromolecules* **2001**, *34*, 8978–8985.